



Micro ceramic fuel cells with multilayered yttrium-doped barium cerate and zirconate thin film electrolytes



Kiho Bae^{a,b}, Dong Young Jang^a, Ho Jean Jung^a, Jun Woo Kim^a, Ji-Won Son^{b,*},
Joon Hyung Shim^{a,**}

^a Renewable Energy System Laboratory, School of Mechanical Engineering, Korea University, 145 Anam-ro, Seongbuk-gu, Seoul 136-701, South Korea

^b High-temperature Energy Materials Research Center, Korea Institute of Science and Technology (KIST), Hwarangno 14-gil 5, Seongbuk-gu, Seoul 136-791, South Korea

HIGHLIGHTS

- Multilayered electrolytes composed of nanoscale BCY/BZY were evaluated in micro-PCFCs.
- The bare BCY PCFC exhibited the highest power but rapidly degraded.
- The BZY capping on BCY did not improve the stability but merely inactivated the cell.
- The cell with BCY-capped BZY marked reasonably high power exhibiting good stability.

ARTICLE INFO

Article history:

Received 20 August 2013

Received in revised form

26 September 2013

Accepted 14 October 2013

Available online 23 October 2013

Keywords:

Micro-protonic ceramic fuel cell

Yttrium-doped barium zirconate

Yttrium-doped barium cerate

Multilayer electrolyte

Pulsed laser deposition

ABSTRACT

Multi- and mono-layered thin film electrolytes based on $\text{BaCe}_{0.9}\text{Y}_{0.1}\text{O}_{3-\delta}$ (BCY) and $\text{BaZr}_{0.85}\text{Y}_{0.15}\text{O}_{3-\delta}$ (BZY) ceramics are fabricated by pulsed laser deposition (PLD) for use in micro-protonic ceramic fuel cells (micro-PCFCs), and their microstructure and fuel cell performances are investigated. Fully dense and well-crystallized BCY and BZY layers are identified in the multi- and mono-layered electrolytes, and are confirmed by microstructural analyses. Fuel cell and impedance measurements confirm that the bare BCY cells exhibit superior performance to samples with BZY capping; however, this capping does not offer any advantage in terms of operational stability. In contrast, the BCY-capped BZY cell performs better than the bare BZY cell, implying that BCY possesses more active surface kinetics. Anodic improvement is as important as cathodic modification for the intermediate-temperature operation of PCFCs. The BCY-capped BZY cell also demonstrates excellent stability, maintaining a good open circuit voltage for over 10 h.

© 2013 Elsevier B.V. All rights reserved.

1. Introduction

Solid oxide fuel cells (SOFCs) have attracted attention as next-generation electrical power generators because of their high conversion efficiency when utilized in a heat–electricity cogeneration system and their stability, which are attributed to their chemically inert ceramic compositions [1]. Conventional SOFCs, however, require high operating temperatures (800–1000 °C) to gain sufficient energy, mostly used for the reduction of O_2 gas into oxide ions on the cathode, and the migration of ions through the electrolyte [1,2]. In particular, SOFCs use oxide ion-conducting electrolytes,

where the low mobility and high activation energy of oxide ions significantly contribute to the ohmic energy loss during the operation [2]. To reduce this ohmic loss, and ultimately reduce the operating temperatures, many attempts have been made to either fabricate ultra-thin electrolytes ($<1\ \mu\text{m}$) [3–7] or to switch to novel ceramic electrolyte materials that exhibit high ionic conductivity at intermediate temperatures (ITs, 400–600 °C) [8–15].

Acceptor-doped cubic perovskite-type oxides, in which protons can be transferred through the lattice, are considered to be promising electrolytes for IT-SOFCs because of their relatively high conductivities and low activation energies in the temperature range 400–600 °C [10,16,17]. Among the proton-conducting oxides, yttrium-doped barium zirconate (BZY) and barium cerate (BCY) are the most widely used electrolyte materials, having relatively high solubility in H_2O and good proton conductivity [10]. There are, however, many challenges associated with the practical use of

* Corresponding author. Tel.: +82 2 958 5530; fax: +82 2 958 5529.

** Corresponding author. Tel.: +82 2 3290 3353; fax: +82 2 926 9290.

E-mail addresses: jwson@kist.re.kr (J.-W. Son), shimm@korea.ac.kr (J.H. Shim).

these materials. The strong basicity of BCY results in reaction with H_2O or acidic gases such as CO_2 and decomposition into $Ba(OH)_2$ or $BaCO_3$, and CeO_2 [10,17–19]. Therefore, H_2O formation during fuel-cell operation, and CO_2 generation when hydrocarbon fuels are used, discourage the utilization of bare BCY as an electrolyte, with chemical stability and long-term reliability being serious problems. In contrast, BZY appears to be stable in more severe environments [17,20,21], and displays greater bulk conductivity than BCY [10,22,23]. Poor sinterability of BZY, however, introduces a large number of grain boundaries, which have greater resistance than the bulk material by several orders of magnitude [10,17,21,24,25]. As a result, the cell performance of PCFCs based on bare BZY electrolytes is significantly lower than those based on BCY electrolytes [26,27]. For example, a maximum power output of approximately 800 mW cm^{-2} at 500°C was reported for a Pd-supported thin film BCY cell (electrolyte thickness $<1\text{ }\mu\text{m}$) with an open circuit voltage (OCV) of over 1 V, while the BZY PCFCs provided less than 5 mW cm^{-2} power with an OCV of $<0.1\text{ V}$ in the same cell format [27]. To overcome these drawbacks, a solid-state mixture of BZY and BCY, or $BaY_x(Zr,Ce)_{1-x}O_{3-\delta}$ (BZCY), was proposed, which exhibited reasonably high proton conductivity and good sinterability [14,21,24]. The BZCY cells, however, appeared to decompose to $BaCO_3$ and CeO_2 when exposed to CO_2 or H_2O [17,28,29], indicating that the poor chemical characteristics of BCY were retained.

In this work, various hybrid multilayered electrolytes composed of BZY with a surface capping of BCY, or BCY with BZY capping, were tested from the viewpoint of fuel cell performance (Fig. 1). Considering the refractory nature of BCY to atmospheric CO_2 and moisture, cells with BCY electrolytes surface-protected with BZY were expected to show superior performance. There is, however, a possibility that the BZY capping could inactivate the surface kinetics of BCY, which would be detrimental for IT operation. This speculation is supported by the poor performance of BZY PCFCs compared to BCY-based cells reported by Iijima et al. [27]. Owing to recent advances in microfabrication techniques, ultrathin BZY films (thickness 100–200 nm) have been successfully produced as dense free-standing membranes with a reasonably high fuel cell performance below 500°C [30,31]. Fabrication of the proposed mono- or multilayered BZY/BCY electrolytes in the free-standing micro-cells is attempted herein to more clearly evaluate the roles of BZY and BCY in terms of ion conduction, surface kinetics, and chemical stability, thereby avoiding bulk-level hindrances such as the grain boundary effect across the membrane.

2. Experimental

To fabricate the free-standing multilayered thin film electrolytes, dense BCY and BZY pellets were used as pulsed laser deposition (PLD) targets. A Lambda Physik 248 nm KrF excimer laser with an energy density of 2.5 J cm^{-2} was used to ablate the surface of the targets. Before the deposition, the base pressure was

maintained below $4.0 \times 10^{-3}\text{ Pa}$ in a vacuum chamber, and then oxygen gas was added to achieve a pressure of 6.7 Pa. The substrates were placed 50 mm away from the targets and were heated at 750°C during deposition.

Micropatterned Si_3N_4/Si wafers, used as the PLD substrates, were prepared according to a previously published process [32]. The area of the window pattern was $145\text{ }\mu\text{m} \times 145\text{ }\mu\text{m}$, representing the effective area of the micro-PCFCs. The growth rates of the BZY and BCY pellets were measured to be 0.08 nm/pulse and 0.13 nm/pulse, respectively, for 200-nm-thick electrolytes. In the cases where additional capping layers were required, 20-nm-thick BZY or BCY films were deposited on one or both sides of the electrolytes. The schematics of the six electrolytes deposited by PLD (BCY, BCY/BZY, BZY/BCY/BZY, BZY, BZY/BCY, and BCY/BZY/BCY) are shown in Fig. 1. After the deposition, reactive ion etching (RIE) with CF_4 was conducted to remove the back Si_3N_4 membrane. Porous Pt was then deposited on both sides using direct current (d.c.) sputtering to form the electrodes of the micro-PCFCs. The thickness of the porous Pt electrodes was 100 nm, with a growth rate of 0.03 nm s^{-1} at a background pressure of 12 Pa Ar.

The crystallinities of the mono- and multilayered thin films were characterized using X-ray diffraction (XRD, Rigaku ATX-G). The microstructure was observed using scanning electron microscopy (SEM, FEI XL-30 FEG) and transmission electron microscopy (TEM, Tecnai JEM 2100F). Energy-dispersive spectroscopy (EDS) was conducted simultaneously with the TEM to analyze the elemental compositions of the deposited electrolytes. To compare the fuel cell performances of the micro-PCFCs, current–voltage (I – V) curves and alternating current (a.c.) impedance spectra were collected using the Gamry framework system (Gamry Reference 3000 Potentiostat/Galvanostat/ZRA). The impedance data were obtained using sweeping a.c. frequencies from 10^6 to 1 Hz with a 10 mV magnitude.

3. Results and discussion

The crystallinities of the electrolytes on the Si_3N_4 membrane were analyzed using XRD in the 2θ mode. The X-ray patterns of the crystalline BCY and BZY in all films are shown in Fig. 2. The 2θ crystal orientation peaks of the BCY and BZY monolayers are well-matched with those of the polycrystalline cubic perovskite phases, and serve as a good guideline for the other films. Because of the ultrathin BCY or BZY interlayer on the surface of the electrolyte, the peaks of BCY and BZY were collected simultaneously from the three-layered films of BZY/BCY/BZY and BCY/BZY/BCY. The cross-sectional SEM images of the micro-PCFCs with the BZY/BCY/BZY and BCY/BZY/BCY electrolytes are shown in Fig. 3. A fully densified microstructure with no apparent grain separation can be observed in the electrolyte layer. Good attachment of the porous electrodes to the electrolyte is also confirmed by the SEM images. Similar microstructures can be identified in the single and dual layer samples.

The microstructures of the mono- and multilayered electrolytes were investigated in more detail using TEM. The TEM cross-sectional images of BCY and BZY deposited on Si_3N_4 are shown in Fig. 4(a)–(b). The films exhibit a fully crystallized columnar structure with no separation from the Si_3N_4 layer, implying that the PLD temperature (750°C) was sufficiently high [33]. An unusual layer is evident on the BCY electrolyte (Fig. 4(a)) that cannot be seen in the other images. From the spot-EDS composition analysis, the layer can be identified as Si_3N_4 that was thermally degraded during the fuel cell test. The morphologies of the multilayer electrolytes are shown in Fig. 4(c) and (d), where the apparent physical boundary separating the BCY and BZY layers is shown as dotted lines. The attachment of the two different layers was analyzed in detail using

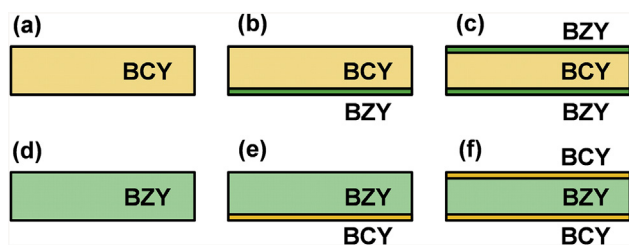


Fig. 1. Schematics of ultrathin mono- or multilayered electrolytes with $BaCe_{0.9}Y_{0.1}O_{3-\delta}$ (BCY) and $BaZr_{0.85}Y_{0.15}O_{3-\delta}$ (BZY) fabricated by pulsed laser deposition (PLD): (a) BCY, (b) BCY/BZY, (c) BZY/BCY/BZY, (d) BZY, (e) BZY/BCY, and (f) BCY/BZY/BCY.

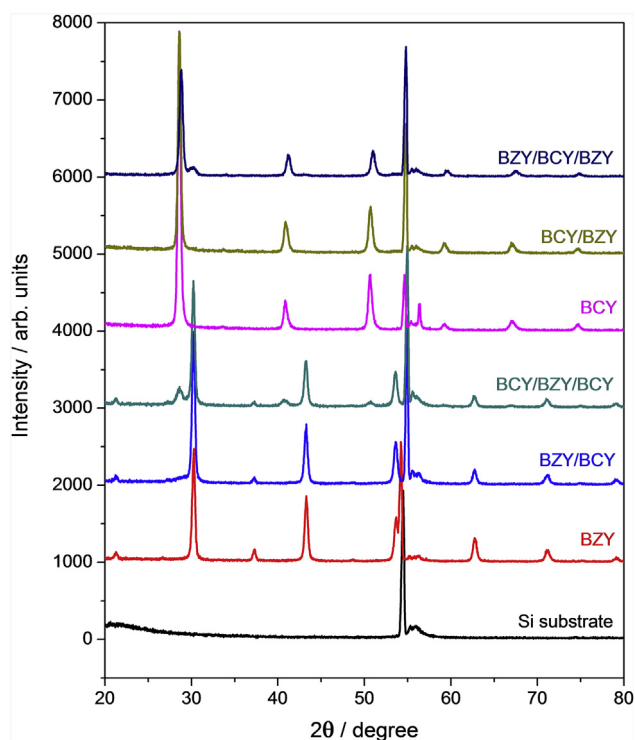


Fig. 2. X-ray diffraction patterns of ultrathin mono- or multilayered electrolytes with $\text{BaCe}_{0.9}\text{Y}_{0.1}\text{O}_{3-\delta}$ (BCY) and $\text{BaZr}_{0.85}\text{Y}_{0.15}\text{O}_{3-\delta}$ (BZY).

high-resolution (HR) TEM imaging. One of the obtained HR-TEM images at the BCY/BZY/BCY interface with Si_3N_4 is shown in Fig. 5. Well-crystallized BCY and BZY layers are clearly evident on the amorphous Si_3N_4 layer. The lattice orientation of the BZY corresponds to that of the BCY, which indicates that the BZY film growth was influenced by the crystal structure of the BCY. This orientation alignment seems to promote good adhesion between the two materials and should, therefore, reduce the resistance to proton conduction across the interface. The composition of the films deposited by PLD is confirmed by the TEM–EDS analysis. The line mapping of the BZY/BCY/BZY obtained from the focused ion beam (FIB) of the epoxy protection layer on the Si_3N_4 –BZY interface is shown in Fig. 6. The composition of the BCY layer (over the distance of 30–160 nm in Fig. 6) agrees closely with the PLD target value, implying that the PLD process is sufficiently reliable. Near the Si_3N_4 surface, a Zr signal appears at a distance of 20 nm, which coincides with a clear drop in the Ce signal. Near the epoxy side, at a distance of 170 nm, the Ba signal rapidly decreases, presumably because of the noise from the epoxy layer.

The fuel cell performances of the micro-PCFCs were evaluated with an apparatus similar to that used in a previous report [32]. Humidified H_2 gas (3% $\text{P}_{\text{H}_2\text{O}}$) was passed through constant-temperature water in a thermostat bath, and then fed into the anode side compartment at a flow rate of $20 \text{ cm}^3 \text{ min}^{-1}$. The cathode side was exposed to ambient air during the operation. The I – V – P plots from the micro-PCFCs with the BCY, BCY/BZY, and BZY/BCY/BZY electrolytes were measured at 400°C (Fig. 7). The bare BCY cell displays the highest maximum power density value 145 mW cm^{-2} with an OCV of 0.98 V, while the BCY/BZY and BZY/BCY/BZY cells show values of 48.1 mW cm^{-2} (OCV 0.89 V) and 8.12 mW cm^{-2} (OCV 0.78 V), respectively. This result clearly indicates that the BZY capping causes deterioration of the fuel cell performance. The electrochemical impedance spectroscopy (EIS) spectra suggest that the power degradation arises because of

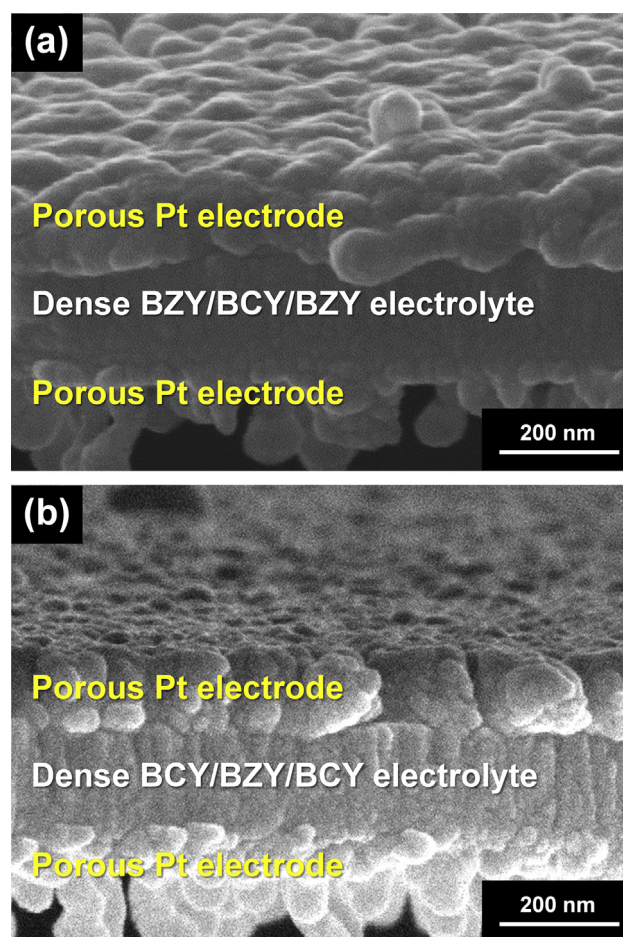


Fig. 3. Cross-sectional scanning electron microscopy images of micro-protonic ceramic fuel cell with multilayered electrolytes of (a) BZY/BCY/BZY and (b) BCY/BZY/BCY. BCY, $\text{BaCe}_{0.9}\text{Y}_{0.1}\text{O}_{3-\delta}$; BZY, $\text{BaZr}_{0.85}\text{Y}_{0.15}\text{O}_{3-\delta}$.

polarization loss, and not ohmic resistance, where the low-frequency impedance spectra correspond to the electrode processes, while the high-frequency arcs represent the electrolyte resistances (Fig. 8). Variations in the impedance of the BCY, BCY/BZY, and BZY/BCY/BZY samples can be identified by their different d.c. bias voltages (0, 0.5, and 0.7 V), with no significant change in the shape or magnitude of the semicircles in the high-frequency range (Fig. S1(a)–(c) in the Supporting information). This confirms that the high-frequency arcs accurately represent the electrolyte impedance. The short-term stabilities of the BCY, BCY/BZY, and BZY/BCY/BZY cells were evaluated by repeated I – V fuel cell measurements. During the intervals between the I – V measurements, the OCV was measured for 10 min (zero-current measurement). The results of the BCY cell measured at 400°C and that of the BZY/BCY/BZY cell at 425°C are shown in Fig. 9. The OCV and power values can be seen to abruptly decrease for both samples, with a similar trend evident for the BCY/BZY cell. It is suspected that this rapid degradation of the BCY-based cells is due to their intrinsic chemical instability and degradation of the BCY [19], despite the 20-nm-thick BZY capping layer providing some protection against atmospheric CO_2 and moisture. At temperatures above 425°C , no meaningful data were collected from the BCY-based cells because of their chemical instability.

The fuel cell performances of the BZY-based micro-PCFCs (BZY, BZY/BCY, and BCY/BZY/BCY) were also compared. The I – V – P data obtained from fuel cell testing at 475°C are shown in Fig. 10. From

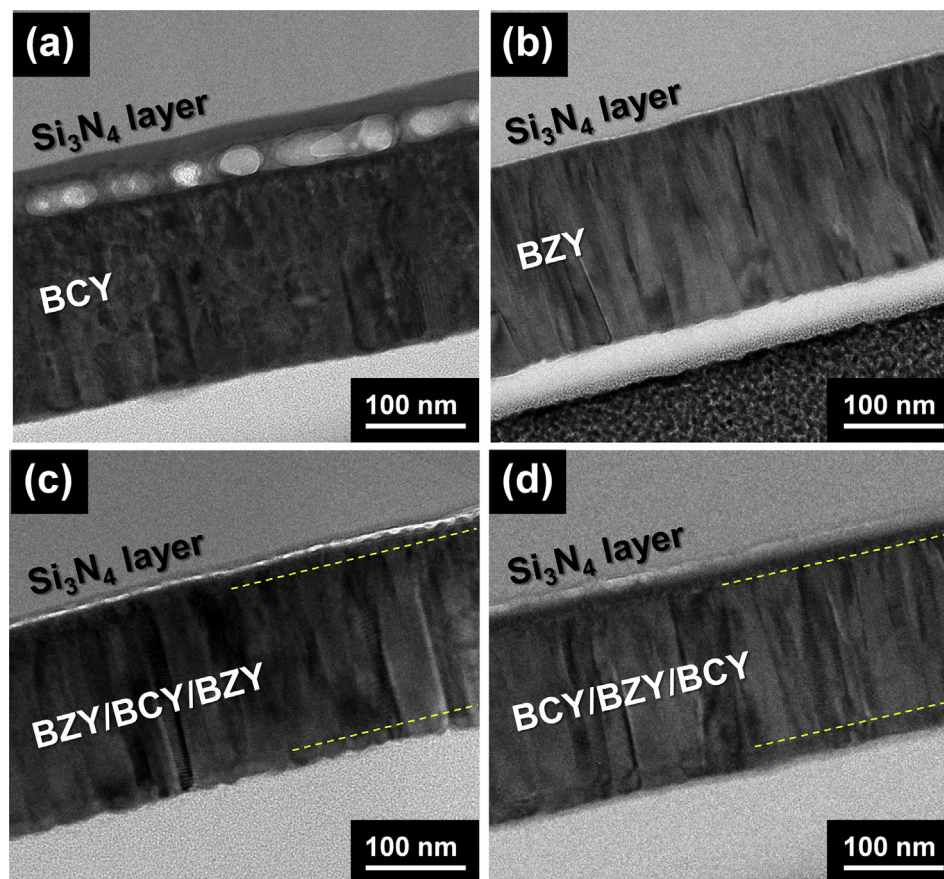


Fig. 4. Cross-sectional transmission electron microscopy images of mono- and multilayered electrolytes: (a) BCY, (b) BZY, (c) BZY/BCY/BZY, and (d) BCY/BZY/BCY. BCY, $\text{BaCe}_{0.9}\text{Y}_{0.1}\text{O}_{3-\delta}$; BZY, $\text{BaZr}_{0.85}\text{Y}_{0.15}\text{O}_{3-\delta}$.

the results, it is clear that the BCY capping layer on the BZY electrolyte enhances the fuel cell performance. The highest maximum power density obtained from the BCY/BZY/BCY sample is 62.3 mW cm^{-2} , with an OCV of 1.05 V. The BZY/BCY, where the

anode side surface of BZY is replaced with BCY, also displays better performance than the bare BZY, with maximum power outputs of 39.6 mW cm^{-2} (OCV 1.06 V) and 27.2 mW cm^{-2} (OCV 1.08 V), respectively. It should be noted that the OCV of the BZY-based cell is relatively high ($\geq 1.05 \text{ V}$) compared to that of the BCY-based cells ($< 1 \text{ V}$). This is presumably because BZY is more effective than BCY in separating the electrode processes. The EIS analysis confirms that this enhancement is due to the reduced polarization resistance, as shown in Fig. 11. The total impedance is also significantly lower for the BCY/BZY/BCY and BZY/BCY samples compared to that for the BZY cell. The same method used in the BCY-based micro-PCFCs was also employed to evaluate the semicircles in the high-frequency range representing the ohmic resistance (Fig. S2(a)–(c)).

To evaluate the stability of the BCY interlayer during the fuel cell operation, the BCY/BZY/BCY cell was measured at 400°C for 10 h, as shown in Fig. 12. In contrast to the BCY-based micro-PCFCs, the BZY-based samples show a stable OCV, greater than 1 V, for the entire testing time (see Fig. 9). During the initial measurement period of 2.5 h, the OCV remains close to 1.1 V. On applying a current loading of 50 mA cm^{-2} for 1.8 h, the cell voltage decreases slightly from 0.69 to 0.66 V, and undergoes some fluctuation. After the current loading period, the second OCV measurement was conducted for approximately 2.7 h. In this second period, a slightly lower OCV of 1.04 V is maintained. The second current loading test was then conducted with a current density of 100 mA cm^{-2} for 1.3 h. During this period, a cell voltage drop from 0.45 to 0.39 V is observed, which is larger than that seen in the first loading test. After the second loading test, a slightly lower OCV of approximately 1.0 V is evident, but remains reasonably high ($> 0.98 \text{ V}$) during the last test period of approximately 1.7 h. Although a slight degradation of the performance

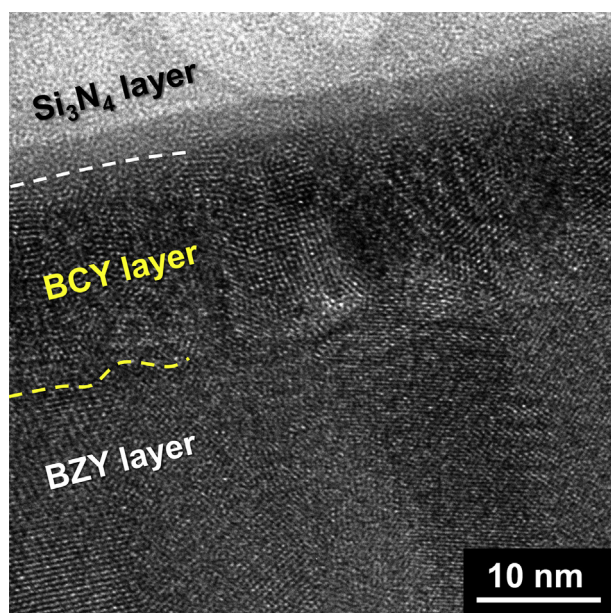


Fig. 5. Cross-sectional high-resolution transmission electron microscopy image at the interface on the anode side of the BCY/BZY/BCY multilayered electrolyte. BCY, $\text{BaCe}_{0.9}\text{Y}_{0.1}\text{O}_{3-\delta}$; BZY, $\text{BaZr}_{0.85}\text{Y}_{0.15}\text{O}_{3-\delta}$.

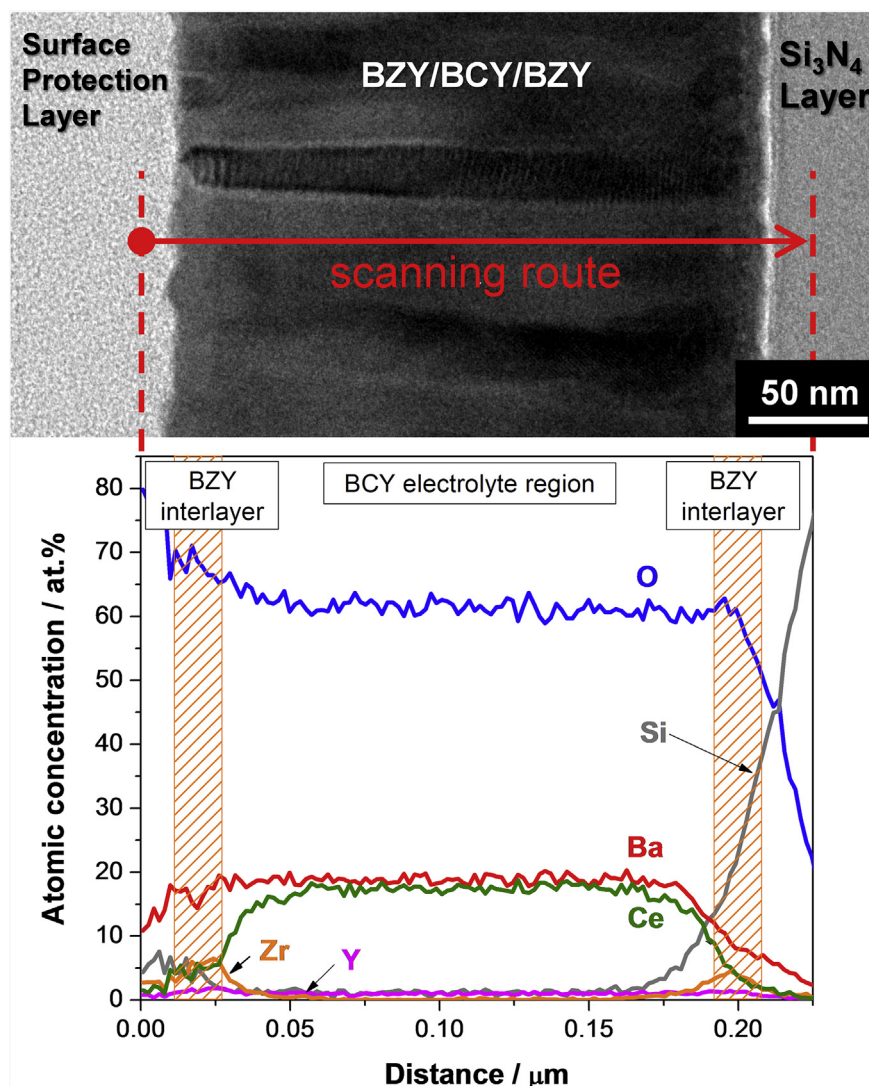


Fig. 6. Line mapping compositional analysis of BZY/BCY/BCY multilayered electrolyte obtained using transmission electron microscopy–energy-dispersive spectroscopy. BCY, $\text{BaCe}_{0.9}\text{Y}_{0.1}\text{O}_{3-\delta}$; BZY, $\text{BaZr}_{0.85}\text{Y}_{0.15}\text{O}_{3-\delta}$.

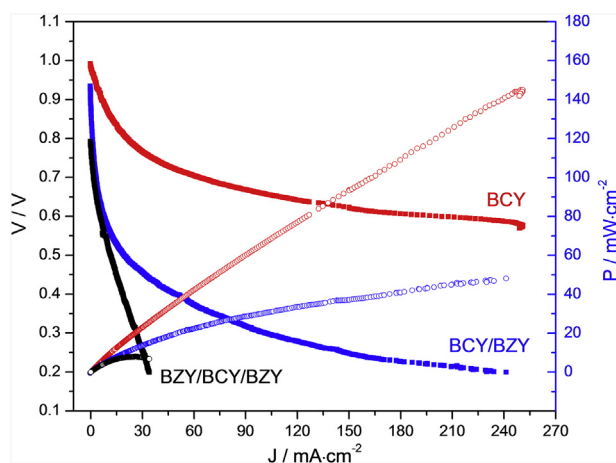


Fig. 7. Current–voltage–power (I – V – P) comparison of BCY-based micro-protonic ceramic fuel cells with BCY, BCY/BZY, and BZY/BCY/BZY electrolytes at an operating temperature of 400 °C under air/wet H_2 gas conditions. BCY, $\text{BaCe}_{0.9}\text{Y}_{0.1}\text{O}_{3-\delta}$; BZY, $\text{BaZr}_{0.85}\text{Y}_{0.15}\text{O}_{3-\delta}$.

occurs during the two current loading periods, the BCY/BZY/BCY PCFC performance is highly stable, and in particular, is superior to that of the BCY-based cells, i.e., the bare BCY and the BZY/BCY/BZY cells. It is suspected that the slight performance degradation is mainly due to the thermally weak and porous Pt electrodes, as reported in previous studies on sputtered porous Pt conducted in a setup similar to that used in the present work [34–36].

The main factors affecting the polarization resistance are gas infiltration to the reactive surface such as the triple phase boundary (TPB), and the surface kinetics at the electrolyte/electrode interface or on the surfaces of the electrode or electrolyte. Because the Pt layer is only ~100 nm thick and has a porous structure, as confirmed in the SEM images, the gas diffusion into the TPB may not be a critical factor in the polarization impedance. Considering that the gas and O^{2-}/H^+ solubility in Pt is negligible, the surface-exchange process on the electrode surface may also be ignored. Therefore, the reaction kinetics at the interface between the electrode and the electrolyte seems to be the rate-determining step of the overall polarization process. In this respect, the improved fuel cell performance of the multilayer electrolytes can be explained by the superior surface kinetics of BCY compared to BZY. The larger

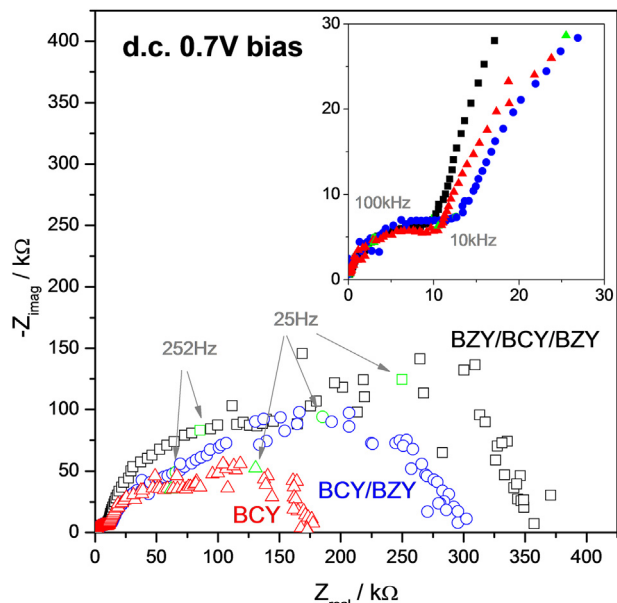


Fig. 8. Electrochemical impedance spectroscopy comparison of BCY-based micro-protonic ceramic fuel cells with BCY, BCY/BZY, and BZY/BCY/BZY electrolytes at an operating temperature of 400 °C under air/wet H₂ gas conditions. BCY, BaCe_{0.9}Y_{0.1}O_{3-δ}; BZY, BaZr_{0.85}Y_{0.15}O_{3-δ}. d.c., direct voltage.

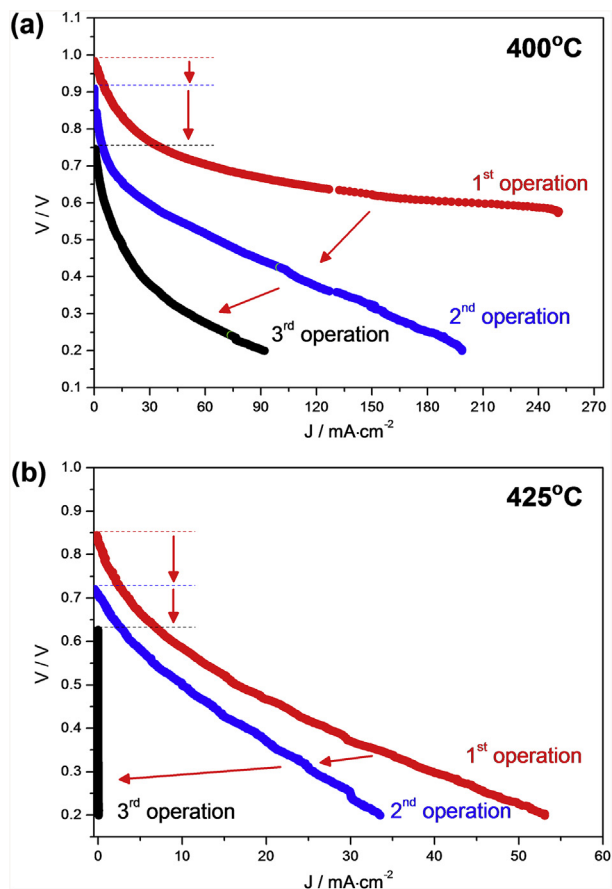


Fig. 9. Results of repeated fuel cell testing of (a) BCY and (b) BZY/BCY/BZY micro-protonic ceramic fuel cells (micro-PCFCs), showing rapid degradation of fuel cell performance along with a drop in open circuit voltage (OCV). BCY, BaCe_{0.9}Y_{0.1}O_{3-δ}; BZY, BaZr_{0.85}Y_{0.15}O_{3-δ}.

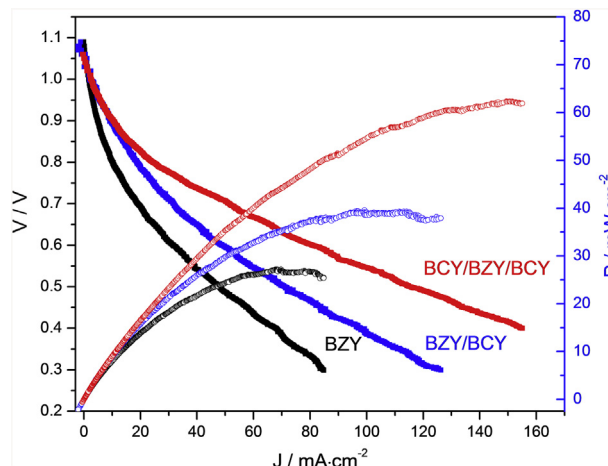


Fig. 10. Current–voltage–power (*I–V–P*) comparison of BZY-based micro-protonic ceramic fuel cells with BZY, BZY/BCY, and BCY/BZY/BCY electrolytes at an operating temperature of 475 °C under air/wet H₂ gas conditions. BCY, BaCe_{0.9}Y_{0.1}O_{3-δ}; BZY, BaZr_{0.85}Y_{0.15}O_{3-δ}.

interface resistance of BZY in comparison to BCY has also been previously reported [21,37]. Fabbri et al. [21] showed that the polarization resistance increased with increasing Zr content in BCZY electrolytes. They also identified an increase in the cathodic polarization when a BZY protective layer (thickness 2–3 μm) was deposited onto the BCY electrolyte [37]. The results obtained in the present study confirm that the shallow BCY surface capping also significantly enhances the fuel cell performance, as shown in Fig. 10 (230% improvement in terms of the maximum power output). The good stability of the BZY is also preserved, as demonstrated in the repeated testing of the BCY/BZY/BCY cell (see Fig. 12). It is also noteworthy that the anodic polarization significantly affects the PCFC performance, as confirmed from the comparison of the bare BCY and BCY/BZY cells (see Fig. 7), and the bare BZY and BZY/BCY cells (see Fig. 10).

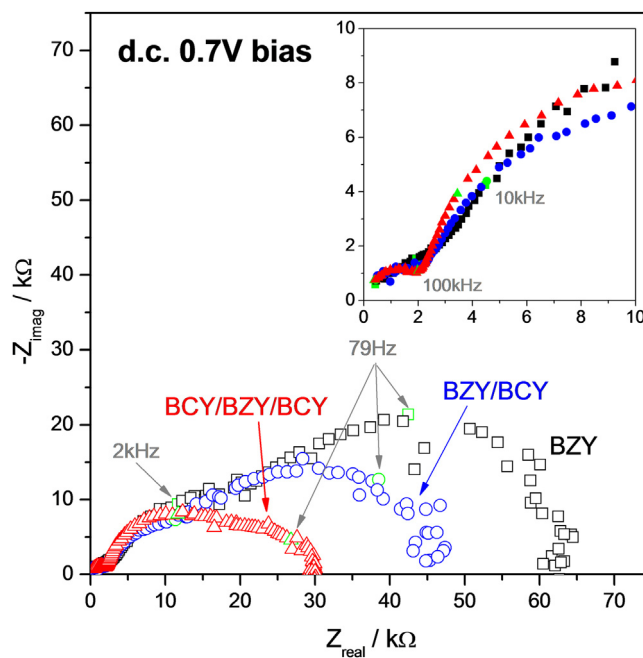


Fig. 11. Electrochemical impedance spectroscopy comparison of BZY-based micro-protonic ceramic fuel cells with BZY, BZY/BCY, and BCY/BZY/BCY electrolytes at an operating temperature of 475 °C under air/wet H₂ gas conditions. BCY, BaCe_{0.9}Y_{0.1}O_{3-δ}; BZY, BaZr_{0.85}Y_{0.15}O_{3-δ}. d.c., direct current.

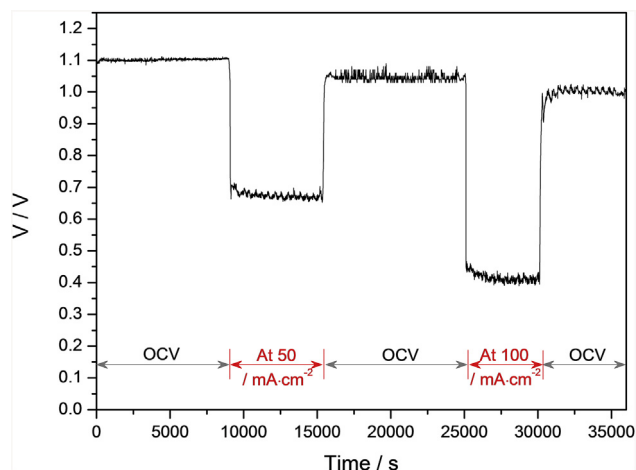


Fig. 12. Durability tests of BCY/BZY/BCY micro-protonic ceramic fuel cells (micro-PCFCs) for 10 h at an operating temperature of 400 °C using a galvanostatic method. BCY, $\text{BaCe}_{0.9}\text{Y}_{0.1}\text{O}_{3-\delta}$; BZY, $\text{BaZr}_{0.85}\text{Y}_{0.15}\text{O}_{3-\delta}$.

4. Conclusions

In this work, various mono- and multilayered electrolytes composed of BCY and BZY are investigated for use in micro-PCFCs. In particular, a 20-nm-thick BZY capping is introduced onto either the anode, or both the anode and cathode sides of the BCY. Cells based on BZY are also studied, with a 20-nm-thick BCY capping on the anode, or both the anode and cathode sides of the BZY. The total electrolyte thickness is fixed at 200 nm. The films are deposited by PLD at 750 °C, and well-crystallized and fully densified electrolytes can be observed in the XRD and SEM results. The TEM and EDS analyses reveal a fully crystallized columnar structure with good adhesion between the layers and a stoichiometric composition of BCY and BZY in both the mono- and multilayered electrolytes. The highest power output occurs from the bare BCY PCFC (145 mW cm^{-2} , OCV of 0.98 V) at 400 °C; however, a rapid degradation in power with a significant drop in the OCV is also apparent. The results indicate that the BZY surface capping does not help improve the stability; it merely inactivates the BCY surface. In contrast, BCY-capping significantly enhances the power performance when incorporated in BZY-based cells. For example, the BCY/BZY/BCY cell produces a maximum power of 62.3 mW cm^{-2} at 475 °C, while the bare BZY cell produces only 27.2 mW cm^{-2} power at the same temperature. Good stability of BCY/BZY/BCY is evident from the OCV results from the experiments that include periodic current interruptions over a period of 10 h. Enhanced surface kinetics of BCY compared to BZY are clearly confirmed by the comparison of the I – V and EIS data, especially regarding the differences between the bare BCY and BZY/BCY/BZY cells, and the bare BZY and BCY/BZY/BCY cells. It is interesting that the BCY anodic capping also significantly improves the fuel cell performance. This suggests that the introduction of the BCY capping on both the anode and cathodes sides can further improve the power performance of BZY- or BCZY-based PCFCs by preserving their long-term stability.

5. Glossary

a.c., alternating current; BCY, $\text{BaCe}_{0.9}\text{Y}_{0.1}\text{O}_{3-\delta}$; BZCY, $\text{BaY}_x(\text{Zr,Ce})_{1-x}\text{O}_{3-\delta}$; BZY, $\text{BaZr}_{0.85}\text{Y}_{0.15}\text{O}_{3-\delta}$; d.c., direct current; EDS, energy-dispersive spectroscopy; EIS, electrochemical impedance spectroscopy; FIB, focused ion beam; HR, high-resolution; I – V , current–voltage; IT, intermediate temperature; micro-PCFC, micro-protonic ceramic fuel cell; OCV, open circuit voltage; PLD, pulsed laser deposition; RIE, reactive ion etching; SEM, scanning electron

microscopy; SOFC, solid oxide fuel cell; TEM, transmission electron microscopy; TPB, triple phase boundary; XRD, X-ray diffraction.

Acknowledgments

The authors are grateful to the Fusion Research Program for Green Technologies of the National Research Foundation (NRF) of Korea funded by the Ministry of Education, Science, and Technology (MEST) (Grant No. NRF-2011-0019300), and to the Young Fellow Program of Korea Institute of Science and Technology (KIST) for financial support.

Appendix A. Supplementary data

Supplementary data related to this article can be found at <http://dx.doi.org/10.1016/j.jpowsour.2013.10.057>.

References

- [1] S.C. Singhal, *Solid State Ionics* 152 (2002) 405–410.
- [2] B.C.H. Steele, A. Heinzel, *Nature* 414 (2001) 345–352.
- [3] S. de Souza, S.J. Visco, L.C. De Jonghe, *Solid State Ionics* 98 (1997) 57–61.
- [4] P.C. Su, C.C. Chao, J.H. Shim, R. Fasching, F.B. Prinz, *Nano Lett.* 8 (2008) 2289–2292.
- [5] D. Beckel, A. Bieberle-Hütter, A. Harvey, A. Infortuna, U.P. Muecke, M. Prestat, J.L.M. Rupp, L.J. Gauckler, *J. Power Sources* 173 (2007) 325–345.
- [6] A. Evans, A. Bieberle-Hütter, J.L.M. Rupp, L.J. Gauckler, *J. Power Sources* 194 (2009) 119–129.
- [7] J.H. Shim, C.-C. Chao, H. Huang, F.B. Prinz, *Chem. Mater.* 19 (2007) 3850–3854.
- [8] S.M. Haile, *Acta Mater.* 51 (2003) 5981–6000.
- [9] H. Iwahara, T. Esaka, H. Uchida, N. Maeda, *Solid State Ionics* 3–4 (1981) 359–363.
- [10] K.D. Kreuer, *Annu. Rev. Mater. Res.* 33 (2003) 333–359.
- [11] A.M. Azad, S. Larose, S.A. Akbar, *J. Mater. Sci.* 29 (1994) 4135–4151.
- [12] J.P.P. Huijsmans, F.P.F. van Berkel, G.M. Christie, *J. Power Sources* 71 (1998) 107–110.
- [13] H. Iwahara, Y. Asakura, K. Katahira, M. Tanaka, *Solid State Ionics* 168 (2004) 299–310.
- [14] C. Zuo, S. Zha, M. Liu, M. Hatano, M. Uchiyama, *Adv. Mater.* 18 (2006) 3318–3320.
- [15] E.D. Wachsman, K.T. Lee, *Science* 334 (2011) 935–939.
- [16] E. Fabbri, D. Pergolesi, E. Traversa, *Chem. Soc. Rev.* 39 (2010) 4355–4369.
- [17] E. Fabbri, L. Bi, D. Pergolesi, E. Traversa, *Adv. Mater.* 24 (2012) 195–208.
- [18] K.D. Kreuer, *Solid State Ionics* 97 (1997) 1–15.
- [19] S.V. Bhide, A.V. Virkar, *J. Electrochem. Soc.* 146 (1999) 2038–2044.
- [20] P. Babilo, S.M. Haile, *J. Am. Ceram. Soc.* 88 (2005) 2362–2368.
- [21] E. Fabbri, A. D'Epifanio, E. Di Bartolomeo, S. Licoccia, E. Traversa, *Solid State Ionics* 179 (2008) 558–564.
- [22] E. Fabbri, D. Pergolesi, S. Licoccia, E. Traversa, *Solid State Ionics* 181 (2010) 1043–1051.
- [23] K.D. Kreuer, S. Adams, W. Munch, A. Fuchs, U. Klock, J. Maier, *Solid State Ionics* 145 (2001) 295–306.
- [24] K. Katahira, Y. Kohchi, T. Shimura, H. Iwahara, *Solid State Ionics* 138 (2000) 91–98.
- [25] S.B.C. Duval, P. Holtappels, U.F. Vogt, U. Stimming, T. Graule, *Fuel Cells* 9 (2009) 613–621.
- [26] N. Ito, M. Iijima, K. Kimura, S. Iguchi, *J. Power Sources* 152 (2005) 200–203.
- [27] M. Iijima, N. Ito, S. Matsumoto, S. Iguchi, *MRS Online Proc. Libr.* 972 (2006) AA01–AA08.
- [28] L. Bi, Z. Tao, C. Liu, W. Sun, H. Wang, W. Liu, *J. Membr. Sci.* 336 (2009) 1–6.
- [29] E. Fabbri, L. Bi, H. Tanaka, D. Pergolesi, E. Traversa, *Adv. Funct. Mater.* 21 (2011) 158–166.
- [30] J.H. Shim, J.S. Park, J. An, T.M. Gur, S. Kang, F.B. Prinz, *Chem. Mater.* 21 (2009) 3290–3296.
- [31] Y.B. Kim, T.M. Gur, S. Kang, H.J. Jung, R. Sinclair, F.B. Prinz, *Electrochem. Commun.* 13 (2011) 403–406.
- [32] H. Huang, M. Nakamura, P.C. Su, R. Fasching, Y. Saito, F.B. Prinz, *J. Electrochem. Soc.* 154 (2007) B20–B24.
- [33] Y.B. Kim, T.M. Gur, H.J. Jung, S. Kang, R. Sinclair, F.B. Prinz, *Solid State Ionics* 198 (2011) 39–46.
- [34] J.M. Serra, W.A. Meulenbergh, *J. Am. Ceram. Soc.* 90 (2007) 2082–2089.
- [35] X. Wang, H. Huang, T. Holme, X. Tian, F.B. Prinz, *J. Power Sources* 175 (2008) 75–81.
- [36] Y.B. Kim, C.M. Hsu, S.T. Connor, T.M. Gur, Y. Cui, F.B. Prinz, *J. Electrochem. Soc.* 157 (2010) B1269–B1274.
- [37] E. Fabbri, D. Pergolesi, A. D'Epifanio, E. Di Bartolomeo, G. Balestrino, S. Licoccia, E. Traversa, *Energy Environ. Sci.* 1 (2008) 355–359.